EARTHQUAKE ENGINEERING AND STRUCTURAL DYNAMICS
Earthquake Engng Struct. Dyn. 2010; **39**:751–774
Published online 4 November 2009 in Wiley InterScience (www.interscience.wiley.com). DOI: 10.1002/eqe.972

Column restraint in post-tensioned self-centering moment frames

Chung-Che Chou[1,2,*,†,‡] and Jun-Hen Chen[3,§]

[1]*Department of Civil Engineering, National Taiwan University, Taipei, Taiwan*
[2]*National Center for Research on Earthquake Engineering, Taipei, Taiwan*
[3]*Department of Civil Engineering, National Chiao Tung University, Hsinchu, Taiwan*

SUMMARY

Gaps between beam-to-column interfaces in a post-tensioned (PT) self-centering frame with more than one column are constrained by columns, which causes beam compression force different from the applied PT force. This study proposes an analytical method for evaluating column bending stiffness and beam compression force by modeling column deformation according to gap-openings at all stories. The predicted compression forces in the beams are validated by a cyclic analysis of a three-story PT frame and by cyclic tests of a full-scale, two-bay by first-story PT frame, which represents a substructure of the three-story PT frame. The proposed method shows that compared with the strand tensile force, the beam compression force is increased at the 1st story but is decreased at the 2nd and 3rd stories due to column deformation compatibility. The PT frame tests show that the proposed method reasonably predicts beam compression force and strand force and that the beam compression force is 2 and 60% larger than the strand force with respect to a minor restraint and a pin-supported boundary condition, respectively, at the tops of the columns. Therefore, the earlier method using a pin-supported boundary condition at upper story columns represents an upper bound of the effect and is shown to be overly conservative for cases where a structure responds primarily in its first mode. The proposed method allows for more accurate prediction of the column restraint effects for structures that respond in a pre-determined mode shape which is more typical of low and mid-rise structures. Copyright © 2009 John Wiley & Sons, Ltd.

Received 21 September 2008; Revised 21 September 2009; Accepted 25 September 2009

KEY WORDS: post-tensioned self-centering frame; frame expansion; cyclic frame test; cyclic analysis; column deformation compatibility

1. INTRODUCTION

A post-tensioned (PT) self-centering moment frame that uses post-tensioning steel to compress steel beams against columns has been developed as an alternative to the steel special moment-resisting

*Correspondence to: Chung-Che Chou, Department of Civil Engineering, National Taiwan University, Taipei, Taiwan.
†E-mail: cechou@ntu.edu.tw
‡Associate Professor of Civil Engineering, Associate Research Fellow of National Center for Research on Earthquake Engineering.
§Graduate Student Researcher.

Contract/grant sponsor: National Center of Research on Earthquake Engineering (NCREE)

frame (SMRF). Many researchers have experimentally validated the self-centering behaviors of PT connections with either energy yielding or friction damped devices. Ricles *et al.* [1] first confirmed that an SMRF with PT connections subjected to earthquake records exceed the performance of an SMRF with typical welded connections subjected to the same earthquake records. Christopoulos *et al.* [2] proposed the first PT connection with energy-dissipating (ED) bars, eliminating permanent damage of ED devices during cyclic loads. Garlock *et al.* [3] proposed a first design procedure for a PT frame to achieve desired seismic performances under both the design-based and maximum-considered earthquakes.

Although the newly developed PT connection reaches a satisfactory cyclic performance, the issues of slab and column restraints raised by Christopoulos *et al.* [4] and Garlock [5] have been challenging tasks. Chou *et al.* [6] experimentally demonstrated that the presence of a composite slab significantly alters the self-centering hysteretic behavior while the slab does not open with the PT beam at the beam-to-column interface. In order to eliminate this slab-restraining effect, Garlock *et al.* [3, 5] proposed collector beams to transfer floor inertia force to the PT frame and accommodate PT frame expansion by bending collector beams. Kim and Christopoulos [7–9] proposed details along the boundaries of the slabs that allow for the gap-openings to be accommodated. More recently, Chou *et al.* [10] experimentally showed that the PT connection with a continuous composite slab self-centers with low residual deformations as long as negative connection moments provided by slab reinforcements are considered in design. Chou *et al.* [11] also demonstrated similar cyclic responses between a bare PT connection and a composite PT connection with a discontinuous composite slab, which opens freely along with the gap-opening at the beam-to-column interface.

This gap-opening behavior at the beam-to-column interface causes an expansion in a PT frame (Figure 1), where both ends of the beam in each bay are constrained by columns, so the compression force in the beam is affected by this column restraint that opposes the frame expansion. Christopoulos *et al.* [4] outlined this column-restraining effect and suggested a pinned boundary condition (Figure 1) for upper story columns to estimate column bending stiffness. The validity of the column restraint to the beam was confirmed by tests of a 0.45 scale two-bay single-story substructure that was also pin–pin supported at the tops and bottoms of columns [12]. The assumption of pinned boundary conditions represents a simplified estimate that represents an upper bound of this restraining effect and was suggested to account for the worst-case scenario where a structure responds with a high drift at one floor while the drifts in the floors above and below are almost zero. This can be caused by either a soft-story structure or high mode affecting the response of the structure. Note that when the structure responds in its first mode shape (common seismic response for regular low-to-medium rise structures) where all stories have comparable drifts, the restraining effect might be greatly reduced because the columns are pushed out at all floors simultaneously. Therefore, the previously approximate approach [4] is appropriate in cases where more concentrated response occurs at single floor alone and overly conservative in cases where the structure responds in its first mode. This study presents an alternative method for evaluating bending stiffness of columns and compression forces in the beams based on a deformed column shape that matches the gap-opening at each beam-to-column interface (Figure 1). Since it is very difficult to predict all possible deformed shapes of columns that the structure may experience under different types of earthquakes, this study focuses on the restraining effect of columns in a low-rise PT frame. The proposed method requires the structural analysis of the column in a deformed configuration (Figure 1) and the use of formulation derived from deformation compatibility between the beams, beam strands and the columns. In addition, the analytical formulation is validated by a cyclic

DOI: 10.1002/eqe

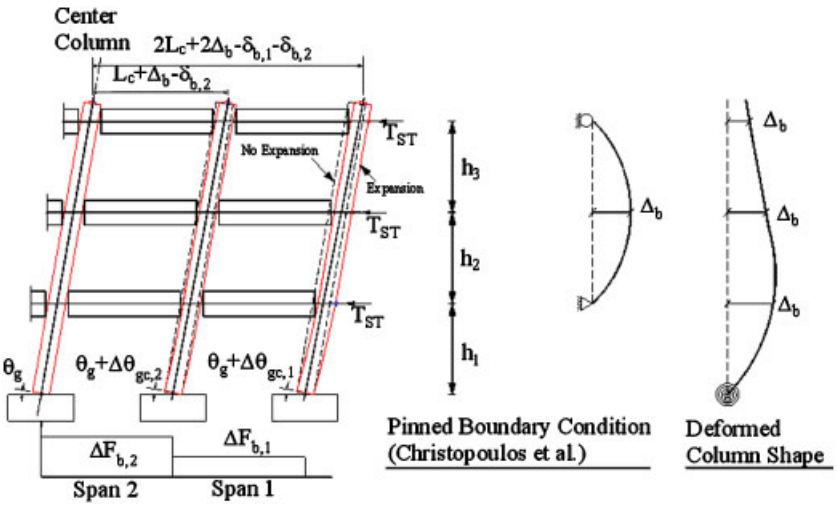

Figure 1. Frame expansion with 2-bay frame.

analysis of a three-story PT frame, which is modeled with numerous axial springs (contact spring, self-centering spring, and ED spring) in connections to capture the gap-opening properties of the frame, and also by cyclic tests of a full-scale, two-bay by first-story PT frame, representing a substructure of the three-story frame. The rotational spring model scheme that includes the behaviors of self-centering, energy dissipation, and column restraint in connections is also presented to capture the PT frame cyclic response.

2. DESIGN OF A THREE-STORY PROTOTYPE BUILDING

2.1. Prototype building

A procedure proposed by Garlock *et al.* [5] was adopted to design a three-story PT prototype frame, which was required to self-center at both seismic hazard levels of the design-based earthquake (DBE) and the maximum considerable earthquake (MCE). Figure 2 shows the plan and elevation of the prototype building, which was assumed to be located on stiff soil in Los Angeles, California. Three two-bay PT frames providing lateral load resistance in the east–west direction were considered in this study; each PT frame was composed of three PT reinforced concrete (RC) columns and PT steel beams. A reduced flange plate (RFP), which is restrained by cover plates to prevent RFP buckling in compression, was proposed by Chou *et al.* [13–15] and incorporated at each beam-to-column connection to increase energy dissipation (Figure 3(a)); no energy dissipation device was used at the PT column base (Figure 3(b)). A concrete slab with metal deck ribs transverse to the east–west beam was adopted, so the slab restraint was insignificant according to the research done by Collins and Filiatrault [16].

The design dead loads were 5.28 kPa (110 psf) and 4.32 kPa (90 psf) for the floors and the roof, whereas the live loads for the floors and the roof were 2.39 kPa (50 psf). Effective seismic weights for the floors and the roof were 2320 and 1896 kN, respectively, resulting in a total seismic weight

DOI: 10.1002/eqe

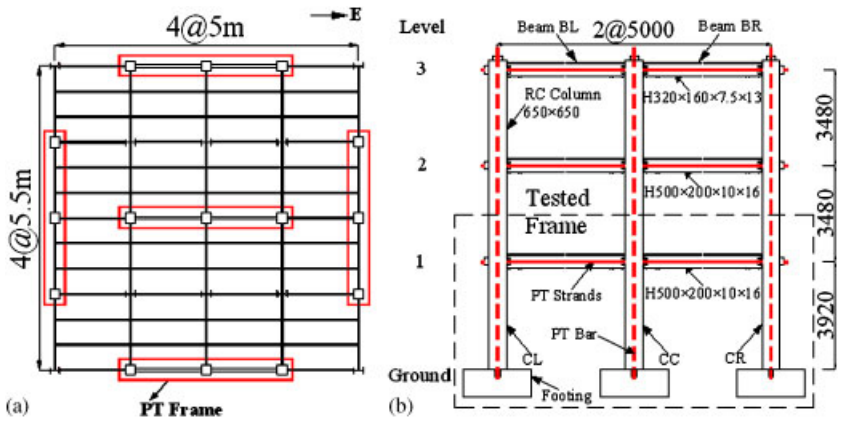

Figure 2. Three-story prototype PT building: (a) plan and (b) elevation.

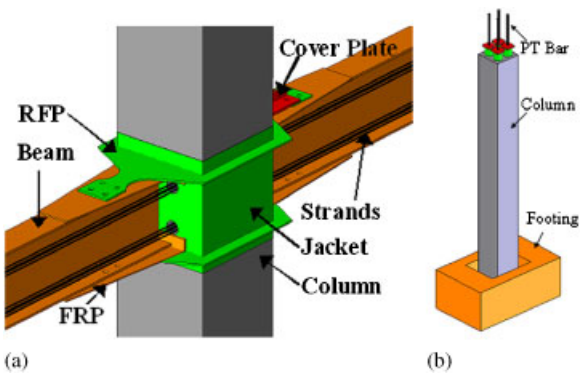

Figure 3. Proposed PT column and connection: (a) PT connection and (b) PT column (no energy-dissipating device).

of the building equal to 6536 kN. The design followed IBC 2000 [17] with a force reduction factor R of 8, an overstrength Ω_0 of 3, and a deflection amplification factor C_d of 5.5. The mapped MCE spectral response acceleration at a short period S_S and one second S_1 was 1.5g and 0.6g, respectively. For the building located at site class D, the site coefficients F_a and F_v were 1.0 and 1.5, respectively, leading to design spectral response accelerations at a short period and one second of 1.0g and 0.6g, respectively. The structural period T and the seismic response coefficient C_s calculated by the codified method were 0.6 s and 0.125, respectively, so the seismic design base shear V_{des} for one PT frame was 272 kN. The selected beam and column sizes, RFP thickness t_R and narrowest dimension b_R, strand and PT bar areas A_{ST}, and initial PT force T_{in} are given in Table I(a). The 650×650-mm RC column containing 12-#11 longitudinal reinforcing bars was stopped near the column base-to-footing interface. The fixity of the column base was provided by four 36-mm diameter high-strength PT bars, which were positioned at the center location, passing through the column base-to-footing interface, and anchored inside the footing. High strength Dywidag (DSI) bar was specified to the PT bar, and ASTM A 706 M steel was specified for the transverse

DOI: 10.1002/eqe

Table I. Prototype frame.

Story	Size	PT element number and size	A_{ST} (mm2)	T_{in} (kN)	t_R (mm)	b_R (mm)	$\frac{M_E}{M_{np}}$	$\frac{M_D}{M_{np}}$	$\frac{M_L}{M_{np}}$	$\frac{M_{\text{dem}}}{M_{np}}$
(a) *Dimension and moment demands*										
3rd	H320 × 160 × 7.5 × 13	12–13 mm Dia.	1184	500	4	120	0.22	0.15	0.09	0.48
2nd	H500 × 200 × 10 × 16	12–13 mm Dia.	1184	900	8	120	0.29	0.05	0.03	0.37
1st	H500 × 200 × 10 × 16	12–15 mm Dia.	1579	900	8	120	0.34	0.05	0.03	0.42
Column	RC 650 × 650	4–36 mm Dia.	4072	1100	—	—	0.24	—	—	0.24

	Decompression			Yield	4% Drift			No column restraint		Column restraint	
Story	$\frac{M_{d,ST}}{M_{np}}$	$\frac{M_{d,R}}{M_{np}}$	$\frac{M_d}{M_{np}}$	$\frac{M_y}{M_{np}}$	$\frac{M_{ST}}{M_{np}}$	$\frac{M_R}{M_{np}}$	$\frac{M_{4\%}}{M_{np}}$	$\frac{P_{4\%}}{\phi_b P_{ry}}$	$\frac{P_{4\%}}{\phi_b P_{ry}} + \frac{M_{4\%}}{\phi_b M_{ry}}$	$\frac{\bar{P}_{4\%}}{\phi_b P_{ry}}$	$\frac{\bar{P}_{4\%}}{\phi_b P_{ry}} + \frac{\bar{M}_{4\%}}{\phi_b M_{ry}}$
(b) *Response in the reinforced beam at column face*											
3rd	0.30	0.070	0.37	0.48	0.65	0.29	0.94	0.21	0.82	0.20	0.8
2nd	0.28	0.072	0.35	0.46	0.56	0.30	0.86	0.25	0.71	0.23	0.69
1st	0.28	0.072	0.35	0.46	0.64	0.29	0.93	0.29	0.80	0.34	0.88
Column	0.2	—	0.2	0.3	—	—	—	—	—	—	—

Floor	α_y	$\alpha_{2\%}$	$\alpha_{4\%}$	α	β
(c) *Moment ratio, post-yielding stiffness ratio, and energy dissipation ratio*					
3rd	1.0	1.2	2.0	0.10	0.8
2nd	1.2	1.7	2.4	0.14	1.0
1st	1.1	1.6	2.2	0.14	1.0

	No column restraint			Column restraint		
Story	$\frac{P_{4\%}}{\phi_b P_{by}}$	$\frac{M_u}{\phi_b M_{by}}$	$\frac{P_{4\%}}{\phi_b P_{by}} + \frac{M_u}{\phi_b M_{by}}$	$\frac{\bar{P}_{4\%}}{\phi_b P_{by}}$	$\frac{\bar{M}_u}{\phi_b M_{by}}$	$\frac{\bar{P}_{4\%}}{\phi_b P_{by}} + \frac{\bar{M}_u}{\phi_b M_{by}}$
(d) *Response in the unreinforced beam at the end of flange reinforcing plates*						
3rd	0.34	0.66	1.0	0.33	0.66	0.99
2nd	0.41	0.49	0.9	0.39	0.49	0.88
1st	0.46	0.54	1.0	0.51	0.57	1.08

Note: M_{ry} = yield moment of the beam plus flange reinforcing plate, P_{ry} = axial strength of the beam plus flange reinforcing plate, $M_{4\%}$ = moment demand at a 4% drift (no column restraint), $P_{4\%}$ = axial load at a 4% drift (no column restraint), $\bar{P}_{4\%}$ = axial load at a 4% drift (with column restraint), $\bar{M}_{4\%}$ = moment demand at a 4% drift (with column restraint), $\phi_b = 0.9$. M_{by} = yield moment of the beam, P_{by} = axial strength of the beam, M_u = moment demand at the end of flange reinforcing plates (no column restraint). $\bar{M}_u$ = moment demand at the end of flange reinforcing plates (with column restraint).

and longitudinal reinforcement. The specified 28-day concrete strength, f'_{cn}, was 28 MPa. A572 Grade 345 (50) steel was used for the steel beams, and ASTM A416 Grade 270 strands were passed along the beam webs and anchored outside the exterior columns CL and CR (Figure 2). Moment demands at the beam-to-column interface and the column base due to seismic design load (M_E), dead load (M_D), and live load (M_L) are also given in Table I(a). The code-based design

DOI: 10.1002/eqe

moment in a combination of these loading sources was M_{dem}, less than $0.55\,M_{np}$, where M_{np} was the beam nominal plastic moment capacity (neglecting the flange reinforcing plate contribution).

The decompression moment of the PT connection M_d (Table I(b)) was composed of the moments provided by strands $M_{d,ST}$ and RFPs $M_{d,R}$, which was computed based on the axial force (smaller than the yield force) in the RFPs at the onset of gap-opening and the distance between the top and bottom RFPs [10, 13]. The decompression moment was larger than the moments due to dead load and live load and was slightly smaller than the moment demand M_{dem} [3]. It is understood that significant inelastic stiffness occurs at the onset of RFP yielding not gap-opening at the beam-to-column interface. The connection moment at the onset of RFP yielding was M_y, which included moments provided by the initial post-tensioning force in strands and yield forces in RFPs. The connection moment M_y was larger than $\alpha_y M_{\text{dem}}$, where $\alpha_y \geqslant 1.0$ (Table I(c)), indicating the elasticity of the PT frame under the code-based seismic load. On the other hand, the post-yielding stiffness ratio α and the energy dissipation factor β for PT connections (Table I(c)) were within the ranges ($0.1 \leqslant \alpha \leqslant 0.150, 7 \leqslant \beta \leqslant 1.0$) suggested by Kim [7].

Following the connection design procedure proposed by Chou *et al.* [10], the connection moment at a drift of 4%, $M_{4\%}$, reached about $0.9\,M_{np}$ at the column face, $M_R \approx 0.3 M_{np}$ of which was provided by the RFPs and $M_{ST} \approx 0.6 M_{np}$ of which was provided by the strands (Table I(b)):

$$M_{4\%} = M_{ST} + M_R = \left[T_{ST}\left(\frac{d_b}{2} - t_f\right)\right] + \left[T_R\left(d_b + \frac{t_R}{2} + t_p - t_f\right) + C_R\left(\frac{t_R}{2} + t_p + t_f\right)\right] \tag{1}$$

where t_R is the thickness of the RFP; t_p is the thickness of the flange reinforcing plate; t_f is the thickness of the beam flange; d_b is the beam depth; T_{ST} is the strand force, and T_R and C_R are the tensile and compressive forces in the RFPs, respectively. The values calculated by the moment-axial compression interaction equation at the column face and the beam section where the flange reinforcing plates are terminated are listed in Table I(b) and (d), indicating that the steel beam remains elastic up to a 4% drift without considering column restraint. Considering the column restraint in the beam, the values show that the column restraint is significant in the 1st story, increasing the value of axial load-bending moment interaction, and is minor in the upper stories. The procedure for determining this effect will be explained in the following section.

3. MODELLING OF A THREE-STORY PT FRAME

Ricles *et al.* [1] used fiber elements to model the self-centering behavior of the PT connection. To model the gap-opening mechanism, fibers of the beam near the beam-to-column interface were characterized by a compression-only stress–strain relationship. The ED device was modeled as an axial spring with a bilinear hysteretic relationship.

Christopoulos *et al.* [4, 9] developed a model with numerous axial springs (ASs) at the PT connection to capture the gap-opening mechanism. This study utilized the connection model proposed by Christopoulos and co-workers [4, 9] to predict the axial load in the beam of the PT frame. Figure 4 illustrates a typical frame incorporating PT connections. The beam and column members were modeled using one-dimensional steel beam–column elements that consist of two nodes, each with three degrees of freedom: the translations in the x and y-directions and the rotation in the z-direction. As can be seen in figure, the elements representing the beams and the column at the beam-to-column interfaces are linked with a number of axial springs to allow for the gap-opening mechanism. Each interior connection requires at least 15 nodes and 20 elements;

DOI: 10.1002/eqe

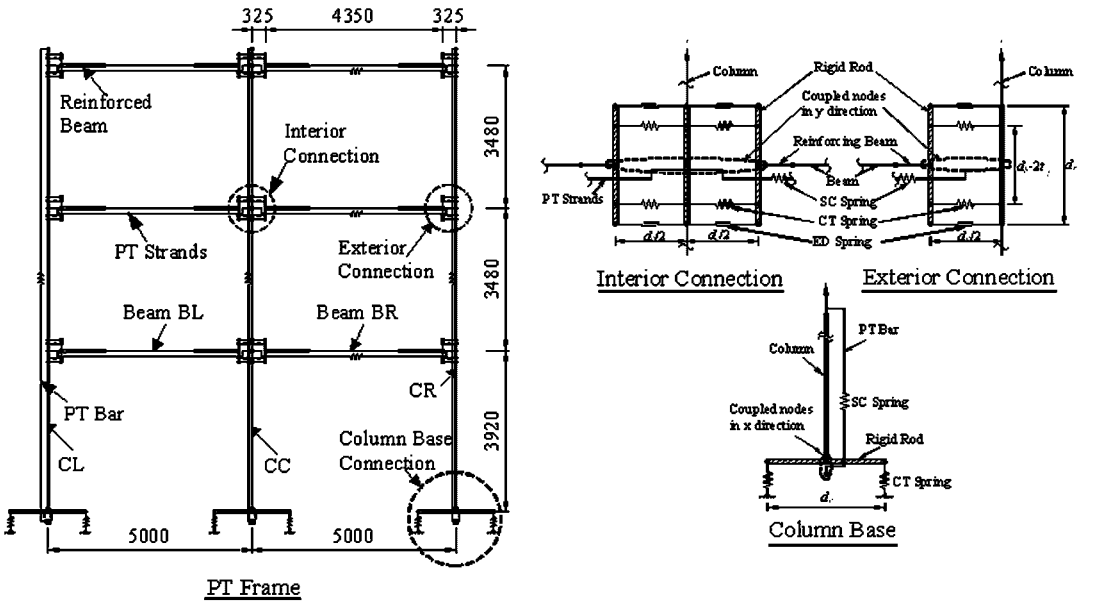

Figure 4. Analytical frame and connection models (AS scheme based on Christopoulos and co-workers [4, 9]).

the elements linked to these nodes are a contact (CT) spring, a self-centering (SC) spring, and an ED spring. The CT spring has high compressive stiffness and near-zero tensile strength to capture the gap-opening mechanism. The SC spring representing the PT strands was modeled as a truss element and anchored to the exterior columns. The ED spring was modeled to capture the energy dissipation of the device. This AS modeling technique could capture the self-centering behavior and the effect of constrained beams in a PT frame. Figures 5(a) and (b) show the monotonic and cyclic force–deformation relationships of the three-story PT frame based on this AS scheme. The analytical model was implemented using the computer program, PISA [18]. The normalized base shear was obtained by dividing the base shear by the value of $V_{\text{des}} = 272\,\text{kN}$. The PT frame first decompressed at the column base (step A) followed by a consecutive gap-opening of the beam-to-column interface at the 3rd, 1st and 2nd stories. The yield strength of the PT frame was 490 kN ($= 1.8\,V_{\text{des}}$) at a roof drift of 0.5%. At a roof drift of 2% (DBE level for the SMRF), the maximum base shear reached $3\,V_{\text{des}}$, and ratio $\alpha_{2\%}$ of beam moment to design moment M_{dem} ranged from 1.2 to 1.7 (Table I(c)). At a roof drift of 4%, ratio $\alpha_{4\%}$ of beam moment to design moment M_{dem} ranged from 2.0 to 2.4. Figure 5(c) shows the expansions of the exterior columns CL and CR, which were computed by subtracting the lateral deformation of the exterior columns by that of the center column CC. The expansion was caused by the gap-opening response at the connection and was more pronounced at the first story than at other stories due to fixity at the base. As can be seen from the analytical results, the compression forces in the 1st-story beams BL (marked as AS(BL)) and BR (marked as AS(BR)) were 10–13% greater than the beam strand force (Figure 6(a)). The compression forces in the 2nd- and 3rd-story beams BL and BR were 2–4 and 7–8%, respectively, smaller than the beam strand force (Figures 6(b) and (c)). Moreover, the compression forces in beams BL and BR at the same story differed.

DOI: 10.1002/eqe

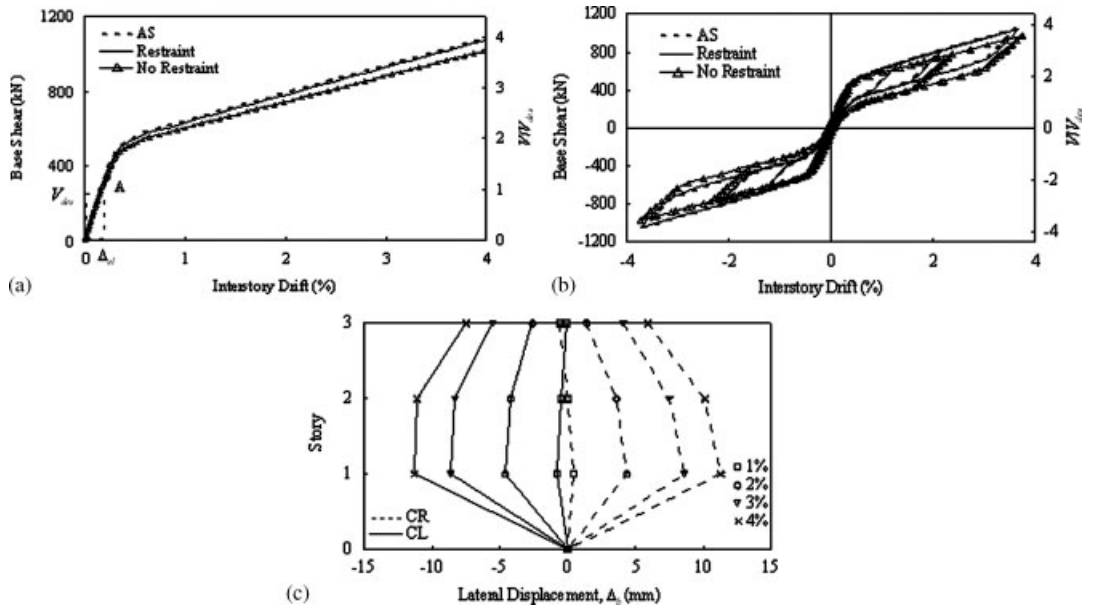

Figure 5. Three-story PT frame response: (a) pushover analysis; (b) cyclic pushover analysis; and (c) column expansion (AS scheme).

4. PREDICTED BEAM COMPRESSION LOAD

4.1. Rotational spring model without including column restraint

Instead of using axial springs at the PT connection, Christopoulos *et al.* [2] proposed a rotational spring scheme to capture the self-centering response of PT connections. This study uses the previously suggested model with a modification in such a way that spring representing the column-restraining effect is computed. Figure 7(a) shows the intersection of the beam and column centerlines with three nodes j, m, and n. Elastic beam–column elements are used to model the beams (lm and no) and the column (ij and jk). Two zero-length spring elements connecting nodes j and m are used to model the bilinear elastic behavior of the PT connection (SC spring) due to gap-opening and the bilinear elastoplastic behavior of the RFP (RFP spring), respectively. The same approach is applied to the node pair j and n. Figure 7(b) shows the relationship between the beam moment and interstory drift θ at the PT connection. The SC spring has the initial elastic rotational stiffness K_{b1} by using a fully restrained moment connection. The inelastic rotational stiffness of the SC spring K_{b2} following decompression is derived by considering a rigid rotation of the PT beam about the beam compression toe. The elastic and inelastic rotational stiffnesses K_{r1} and K_{r2}, respectively, provided by the RFP spring are determined by multiplying the axial stiffness of the RFP and the square of the distance between the beam compression toe and the RFP [13]. A combination of these two rotational springs, which exhibits self-centering and bilinear elastoplastic hysteretic responses, predicts well the experimental results of a PT connection reported elsewhere by Chou *et al.* [10] without the column-restraining effects (Figure 7(c)). Compared with the axial spring (AS) scheme, this rotational spring scheme reduces the number of nodes and elements

DOI: 10.1002/eqe

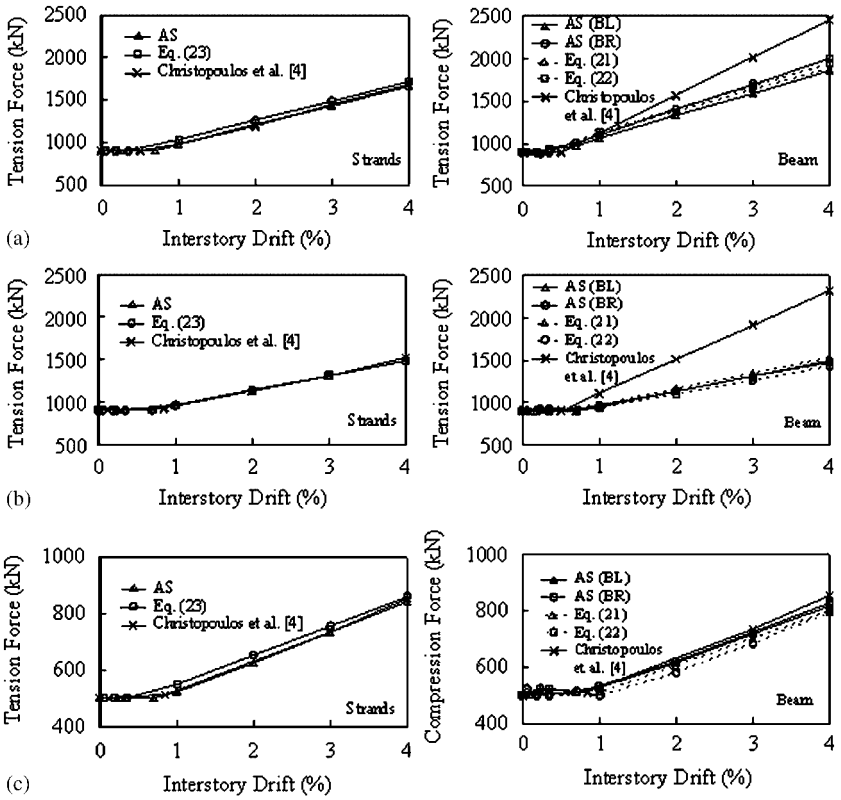

Figure 6. Strand tension force and beam compression force (Three-story PT frame): (a) 1st story; (b) 2nd story; and (c) 3rd story.

required to model the self-centering behavior of the PT connection. However, this simpler approach does not permit to obtain the PT force in the strands and the compression force in the beams.

The rotational spring scheme can also model the self-centering behavior of the PT column. Figure 8(a) shows two nodes j and k at the PT column base. A zero-length rotational spring connecting nodes j and k is used to model the bilinear elastic behavior of the PT column (SC spring). Before decompression, the elastic rotational stiffness of the SC spring K_{c1} is approximated as that of a fully restrained column. After reaching the decompression moment of the PT column $M_{d,c}$ (Figure 8(b)), the rotational stiffness K_{c2} is

$$K_{c2} = \frac{1}{\dfrac{1}{K_{c1}} + \dfrac{1}{K_{\text{cbar}}}} \tag{2}$$

where the rotational stiffness K_{cbar} is provided by the PT force in the column

$$K_{\text{cbar}} = \left[\frac{d_c}{2L_{\text{bar}}} E_{\text{bar}} A_{\text{bar}} \left(1 - \frac{A_{\text{bar}}}{A_{\text{bar}} + A_g}\right)\right] \frac{d_c}{2} \tag{3}$$

DOI: 10.1002/eqe

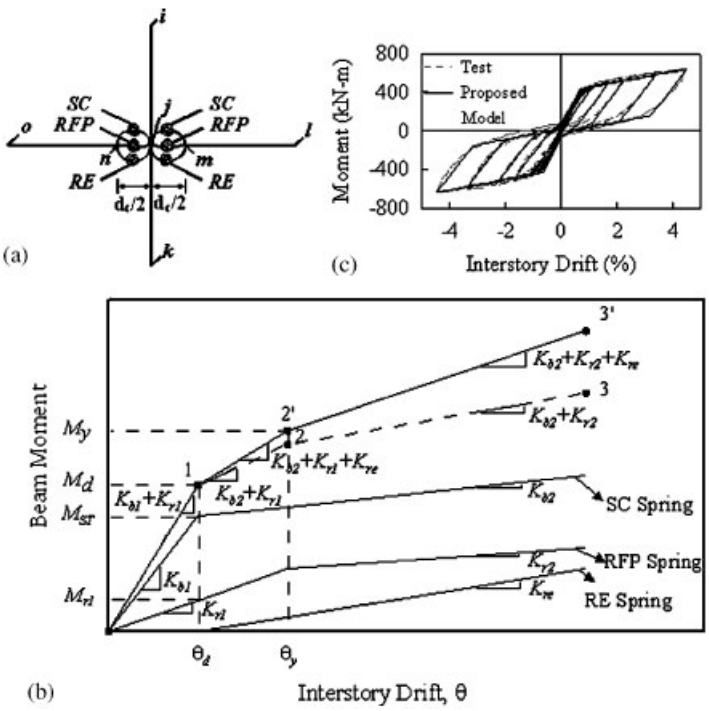

Figure 7. PT connection modeling and prediction comparison: (a) PT connection model; (b) PT connection stiffness; and (c) moment-drift relationship of a connection.

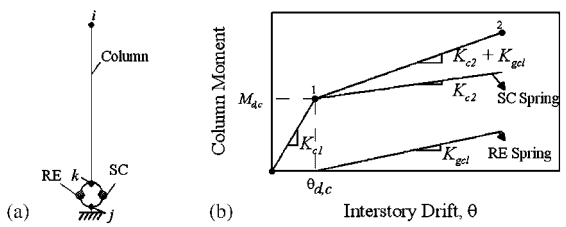

Figure 8. PT column modeling: (a) PT column model and (b) PT column stiffness.

where d_c is the column depth A_{bar} is the PT bar area, L_{bar} is the PT bar length, A_g is the column cross-sectional area and E_{bar} is the elastic modulus of the PT bar. The RE spring and associated stiffness K_{re} and K_{gcl} in Figures 7 and 8 will be discussed in the next section when considering the column restraint.

4.2. Bending stiffness of a PT column based on pinned boundary condition

Figure 9(a) shows a deformed three-story PT frame. As gaps open at the beam-to-column interfaces (Δ_b at each story), the strands along the beams elongate, resulting in axial shortening of the beams

DOI: 10.1002/eqe

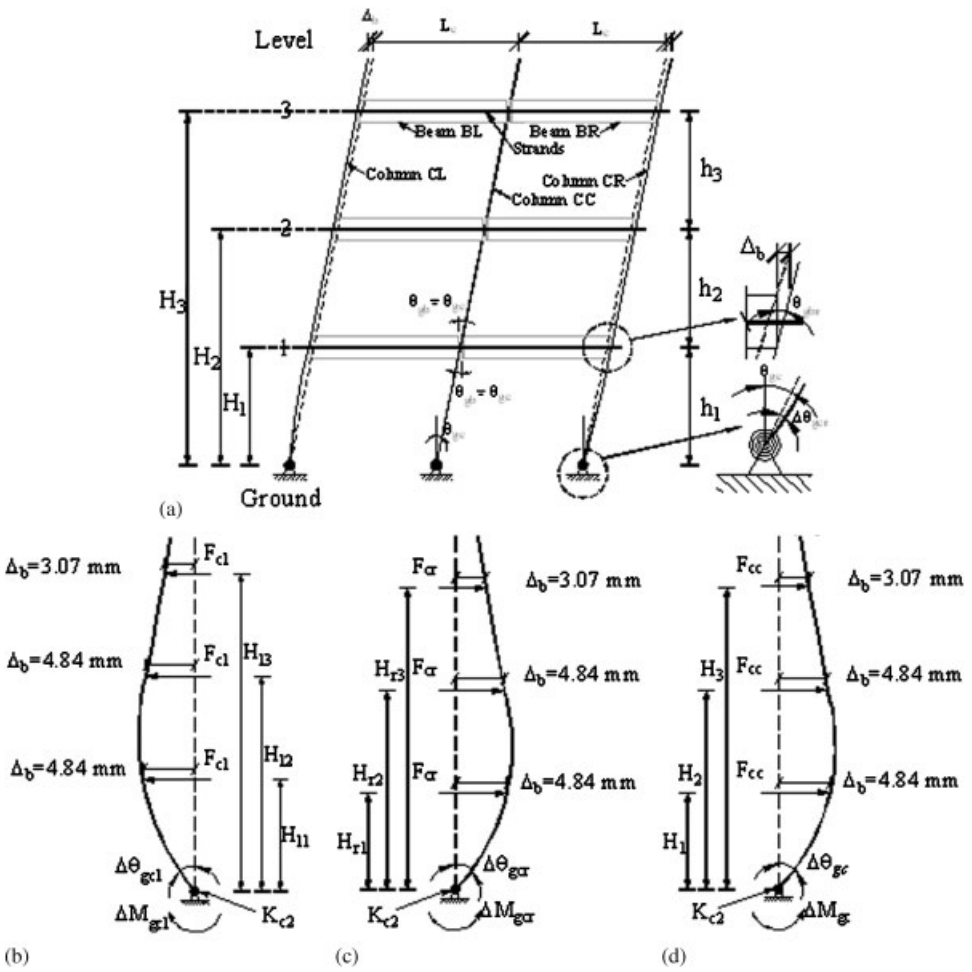

Figure 9. Three-story PT frame and exterior column deformation: (a) PT frame deformation; (b) column CL; (c) column CR; and (d) beam-to-column centerline intersection.

and flexural bending of the exterior columns CL and CR. To determine the bending stiffness of the exterior column K_c at the 2nd story, Christopoulos and co-workers [4, 8] proposed a simple estimation method that assumed the column pin–pin supported at stories above and below the analyzed story. Therefore, the column bending stiffness is

$$K_c = 48\frac{E_c I_c}{(h_2+h_3)^3} \tag{4}$$

where E_c and I_c are the elastic modulus and the moment of inertia of the column, respectively; h_2 and h_3 are the 2nd and 3rd story heights, respectively. For the 1st story, the PT column is assumedly pin-supported at the base with rotational spring stiffness K_{c2} and pin-supported at the

DOI: 10.1002/eqe

2nd story. Thus, the bending stiffness K_c at the 1st story is derived as follows:

$$K_c = \frac{36(h_1+h_2)(E_cI_c)^2 + 12(h_1+h_2)^2 E_cI_cK_{c2}}{12h_1^2h_2^2E_cI_c + h_1^3h_2^2K_{c2}\left(3+\dfrac{h_2}{h_1+h_2}\right)} \tag{5}$$

where h_1 is the 1st story height, and K_{c2} is from Equation (2).

Given that the compression force in the beams along the bays is symmetrical to center column (Figure 1), the increased compression force in the beams due to the PT force and column restraint is [4, 8]:

$$\Delta F_{b,1} = K_b\delta_{b,1} = K_{ST}2\left(n\Delta_b - \sum_{i=1}^{n}\delta_{b,i}\right) + K_c\left(n\Delta_b - \sum_{i=1}^{n}\delta_{b,i}\right) \tag{6}$$

for the beam in the first-bay and by

$$\Delta F_{b,m} = K_b\delta_{b,m} = \Delta F_{b,m-1} + K_c\left[(n-m+1)\Delta_b - \sum_{i=m}^{n}\delta_{b,i}\right] \tag{7}$$

for the beam in the mth bay. The axial compression force applied to the beam in the mth bay is the summation of the initial PT force, T_{in}, and the increased compression force, $\Delta F_{b,m}$. In Equations (6) and (7), $2n$ is the number of bay; $\delta_{b,i}$ is the beam shortening in the ith bay; $K_b(=E_sA_b/L_b)$ is the axial stiffness of the beam, and K_{ST} is the axial stiffness of the strands:

$$K_{ST} = \frac{E_{ST}A_{ST}}{L_{ST}}\left(1 - \frac{A_{ST}}{A_{ST}+A_b}\right) \tag{8}$$

where E_s, A_b and L_b are the elastic modulus, cross-sectional area and length of the steel beam, respectively; E_{ST}, A_{ST} and L_{ST}, are the elastic modulus, cross-sectional area and length of the strands, respectively. Compared with forces obtained from the three-story PT frame model using the AS scheme, this simple approach accurately predicts strand forces but overestimates beam compression forces by 49 and 55% at the 1st and 2nd stories (Figures 6(a) and (b)), respectively, due to the overestimated column bending stiffness.

4.3. Bending stiffness of a PT column based on a deformed column shape

This study utilizes a deformed column shape instead of an assumed pin-supported boundary condition to determine column bending stiffness. The deformed column shape is obtained by considering the following: (1) the gap-opening at each story above the ground level, (2) the beam compression toe position along the column height, and (3) the column base rigidity K_{c2}. Because the positions of the beam compression toe at exterior columns CL and CR differ by a beam depth for any specific frame deformation, the bending stiffnesses provided by the two exterior columns might differ at any drift. Figures 9(b) and (c) show deformed shapes of the two exterior columns CL and CR subjected to gap-openings $\Delta_b(=\theta_g(d_b-t_f))$ at each story. Assuming the same gap-opening angles (i.e. $\theta_g=0.01$ rad.) at the column base and each story, the calculated lateral displacements Δ_b at each story are 4.84, 4.84 and 3.07 mm. Utilizing the computer program PISA [18], column CL has the specified lateral displacement Δ_b at each beam BL top flange inner side, and column CR has the same specified lateral displacement Δ_b at each beam BR bottom flange inner side. The deformed shapes produce incremental rotation angles $\Delta\theta_{\mathrm{gcl}}$ and $\Delta\theta_{\mathrm{gcr}}$ at the bases of columns CL

DOI: 10.1002/eqe

Table II. PT Column bending stiffness.

Story	K_b (kN/m)	K_{ST} (kN/m)	CL	CR		Equations (4) or (5)			
			K_{cl} (kN/m)	K_{cr} (kN/m)	K_{cc} (kN/m)	K_c (kN/m)	$\frac{K_{cl}}{K_c}$	$\frac{K_{cr}}{K_c}$	ς
3rd	305517	18400	−2969	−1986	−2474	0	—	—	1.38
2nd	525195	19643	−2928	−5568	−4193	36849	−0.08	−0.15	1.91
1st	525195	25400	10857	15097	12805	63190	0.17	0.24	0.66

and CR, respectively. The bending stiffnesses of columns CL and CR at each story (K_{cl} and K_{cr}) are computed by dividing the measured reaction forces F_{cl} and F_{cr} by lateral displacements Δ_b. Table II shows that column bending stiffnesses K_{cl} and K_{cr} are different and that ratios K_{cl}/K_c or K_{cr}/K_c are smaller than a unit, indicating that the pin-supported boundary condition significantly increases column bending stiffness. Moreover, negative column bending stiffnesses at the 2nd and 3rd stories indicate that some beam strand tensile forces are needed to deform the column at upper stories to satisfy deformation compatibility so that the beam compression forces are smaller than the beam strand tensile forces.

4.4. Compression load in beams BL and BR

The formulation proposed here follows the one by Christopoulos *et al.* [4] except that (1) a pinned boundary condition in the column is assumed in the previous work and a deformed column shape with consideration of the continuity and boundary condition of columns is utilized in this study, and (2) the effect of column restraint caused by the variation of a beam compression toe under positive and negative bending is illustrated in this study. When the PT frame stays in the original position, the compression force in the beams equals the initial strand force, T_{in}. When the PT frame deforms laterally, the compression force in the beams is contributed by the strands and column restraints. In a deformed frame (Figure 9(a)), the exterior columns CL and CR bear against opposite sides of beams BL and BR, resulting in different column bending stiffnesses (or restraints) at each story (Table II). Incremental equilibrium equations for columns CL and CR at any story (Figure 10) can be determined as follows:

$$\Delta F_{bl} = \Delta F_{cl} + \Delta T_{ST} \tag{9}$$

$$\Delta F_{br} = \Delta F_{cr} + \Delta T_{ST} \tag{10}$$

where ΔF_{bl} and ΔF_{br} are the incremental compression forces in the beams BL and BR, respectively; ΔF_{cl} and ΔF_{cr} are the incremental-restraining forces provided by the columns CL and CR, respectively, and ΔT_{ST} is the incremental strand force. Note that incremental column shear, ΔV_c, above and below the story that is being considered is assumed the same, so it is not considered in the above equations. The shortening in beams BL and BR due to increased compression forces are:

$$\delta_{bl} = \delta_{cl} + \delta_{ST} \tag{11}$$

$$\delta_{br} = \delta_{cr} + \delta_{ST} \tag{12}$$

DOI: 10.1002/eqe

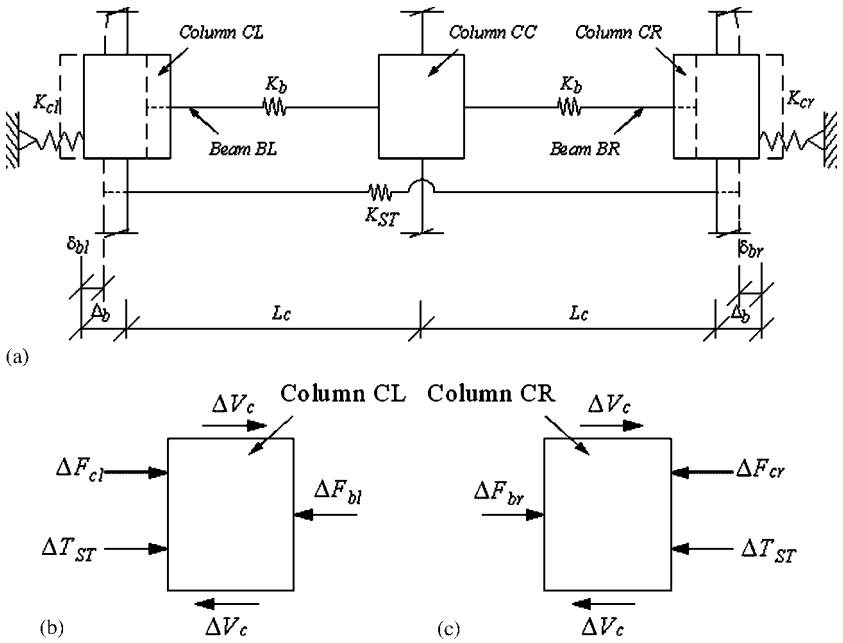

Figure 10. Free-body diagram of columns (based on Christopoulos *et al.* [4]): (a) global relationship; (b) column CL; and (c) column CR.

where δ_{cl} is the beam BL shortening component due to the incremental-restraining force of column CL (ΔF_{cl}); δ_{cr} is the beam BR shortening component due to the incremental-restraining force of column CR (ΔF_{cr}), and δ_{ST} is the beam shortening component due to the incremental strand force ΔT_{ST}.

The incremental-restraining force of column CL is

$$\Delta F_{cl} = K_b \delta_{cl} = K_{cl}(\Delta_b - \delta_{ST} - \delta_{cl}) \tag{13}$$

Equation (13) can be reformulated to determine the shortening in beam BL due to the incremental-restraining force of column CL as follows:

$$\delta_{cl} = \frac{K_{cl}}{K_{cl} + K_b}(\Delta_b - \delta_{ST}) \tag{14}$$

The beam BR shortening due to the incremental-restraining force of column CR can also be expressed as

$$\delta_{cr} = \frac{K_{cr}}{K_{cr} + K_b}(\Delta_b - \delta_{ST}) \tag{15}$$

The deformation ratio between δ_{cr} and δ_{cl} is

$$\varsigma = \frac{\delta_{cr}}{\delta_{cl}} = \frac{K_{cr}(K_{cl} + K_b)}{K_{cl}(K_{cr} + K_b)} \tag{16}$$

DOI: 10.1002/eqe

Since column bending stiffnesses K_{cl} and K_{cr} are different (Table II), the deformation ratio ς is 0.66–1.91 (Table II).

Incremental strand force, ΔT_{ST}, is obtained as follows:

$$\Delta T_{ST} = K_b \delta_{ST} = K_{ST}[2\Delta_b - 2\delta_{ST} - (1+\varsigma)\delta_{cl}] \tag{17}$$

Equation (17) can be reformulated to determine the beam shortening component due to incremental strand force as follows:

$$\delta_{ST} = \frac{K_{ST}}{2K_{ST}+K_b}[2\Delta_b - (1+\varsigma)\delta_{cl}] \tag{18}$$

After substituting Equation (18) into Equations (14) and (15), the beam BL and BR shortening components due to column-restraining forces are:

$$\delta_{cl} = \frac{K_{cl}K_b}{(K_{cl}+K_b)(2K_{ST}+K_b)+(1+\varsigma)K_{ST}K_{cl}}\Delta_b \tag{19}$$

$$\delta_{cr} = \frac{\varsigma K_{cl}K_b}{(K_{cl}+K_b)(2K_{ST}+K_b)+(1+\varsigma)K_{ST}K_{cl}}\Delta_b \tag{20}$$

For any specific gap-opening Δ_b, beam shortenings can be computed using Equations (18)–(20); beam compression forces F_{bl} and F_{br} and strand force T_{ST} are then computed as follows:

$$F_{bl} = T_{in} + \Delta F_{bl} = T_{in} + K_b(\delta_{ST} + \delta_{cl}) \tag{21}$$

$$F_{br} = T_{in} + \Delta F_{br} = T_{in} + K_b(\delta_{ST} + \delta_{cr}) \tag{22}$$

$$T_{ST} = T_{in} + K_b \delta_{ST} \tag{23}$$

Figure 6 shows predictions based on Equations (21)–(23), which are close to forces obtained from the three-story frame model using the AS scheme. The predicted beam compression force is greater than the strand force at the first story and is smaller than the strand force at the second and third stories due to negative column bending stiffnesses (Table II). The beam compression force, which is decreased from the applied strand tensile force at the second and third stories, cannot be obtained by the simple estimation method proposed by Christopoulos and co-workers [4, 8] because the overall column deformation compatibility is not considered in developing column bending stiffness. Table III compares beam compression force at a 4% drift. Although the compression toes in beams BL and BR differ by a beam depth, the column-restraining force variations $K_b\delta_{cl}$ and $K_b\delta_{cr}$ show minor different compared with the value of strand force T_{ST}. For simplicity, the beam-to-column centerline intersection can be used to calculate exterior column bending stiffness. In this case, the column bending stiffness at each story, denoted by K_{cc}, can be computed by reaction force F_{cc} divided by the specified column deformation Δ_b at the beam-to-column interface (Figure 9(d)). The resulting beam compression force is 10% higher than the strand tensile force at the first story and is 2–4% lower than the strand tensile force at the second and third stories (last column in Table III).

4.5. Rotational spring representing column restraint

When gaps open at bases and beam-to-column interfaces, column restraint opposes the frame expansion, varying moments at column bases and connections. To use the rotational spring scheme

DOI: 10.1002/eqe

Table III. Comparison of beam compression force increment and strand tension force (4% drift).

Story	F_{bl} (kN)	F_{br} (kN)	T_{ST} (kN)	$K_b\delta_{cl}$ (kN)	$K_b\delta_{cr}$ (kN)	$K_b\delta_{cc}$ (kN)	$\frac{T_{ST}+K_b\delta_{cl}}{T_{ST}}$ (%)	$\frac{T_{ST}+K_b\delta_{cr}}{T_{ST}}$ (%)	$\frac{T_{ST}+K_b\delta_{cc}}{T_{ST}}$ (%)
3rd	819	826	843	−16	−24	−20	98	97	98
2nd	1474	1485	1489	−76	−40	−58	95	97	96
1st	1866	2008	1666	194	141	167	112	108	110

to capture the cyclic response of a PT frame with column-restraining effects, a third zero-length rotational spring (RE spring in Figure 7(a)) connecting beam nodes j and m is used with rotational stiffness:

$$K_{re}=\frac{K_b\delta_{cc}(d_b/2-t_f)}{\theta_g} \tag{24}$$

where δ_{cc} is the special case of δ_{cl} when $K_{cl}=K_{cc}$ and $\varsigma=1$ in Equation (19). Moment variation at the column base caused by the column restraint is captured by using a rotational spring RE with stiffness K_{gcl} (Figure 8). To reach the specified column shape in Figure 9(d), where a lateral displacement Δ_b at each story is calculated based on θ_g (i.e. $=0.01$ rad.) and the beam depth, the increased moment and the gap-opening angle at the column base are ΔM_{gc} and $\Delta\theta_{gc}$, respectively. The stiffness K_{gcl}, accounting for the increased moment ΔM_{gc} corresponding to the specified gap-opening angle θ_g, is

$$K_{\mathrm{gcl}}=\frac{\Delta M_{gc}}{\theta_g}=\frac{K_{c2}\Delta\theta_{gc}}{\theta_g} \tag{25}$$

Figure 7(b) and Figure 8(b) show that the RE spring has zero rotational stiffness before the gap opens at the beam-to-column interface and the column base. Figures 5(a) and (b) show the effects of column restraints on the monotonic and cyclic responses of the PT frame modeled using the rotational spring scheme. The post-yielding stiffness of the frame with RE springs approximates that using the AS scheme and is 6% larger than that without RE springs. Furthermore, Figure 11 shows the cyclic responses of interior PT connections in the frame model with and without RE springs. Overall cyclic responses in the two models are generally similar. However, including RE springs in the frame model increases moments at the 1st-story connection and slightly decreases moments at the 2nd- or 3rd-story connections. For a PT frame with more than two bays in width, the column bending stiffness K_c obtained from the pinned boundary condition in Equations (6) and (7) is replaced by the column bending stiffness K_{cc} obtained based on the deformed column shape. The beam shortening in the ith bay is expressed by

$$\delta_{b,i}=\delta_{ST}+\sum_{i=1}^{n}\delta_{cc,i} \tag{26}$$

where $\delta_{cc,i}$ is the beam shortening component due to the column restraint δ_{cc} in the ith bay.

DOI: 10.1002/eqe

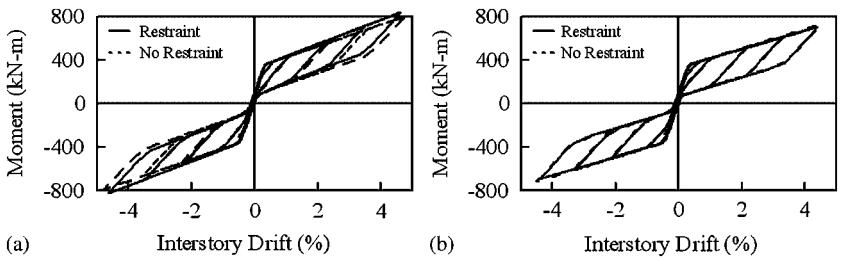

Figure 11. Moment and drift relationships of interior connections (three-story frame): (a) 1st-story and (b) 2nd-story.

4.6. Procedure for assessing column restraint

A step-by-step procedure that is used to assess the column restraint in a low-rise PT self-centering frame is summarized as below:

(1) The initial beam and column sections are sized using the seismic design procedure proposed by Garlock *et al.* [3] or Kim and Christopoulos [8].
(2) A deformed shape of columns is determined in accordance with the specified lateral displacement $\Delta_b[=\theta_g(d_b-t_f)]$ at each story.
(3) Construct a column model with the rotational spring stiffness K_{c2} at the base (Equation (2)) and push out the column to reach the specified lateral displacement at each story. The column bending stiffness K_{cc} at each story is computed by the corresponding reaction force divided by the specified lateral displacement.
(4) Compute beam shortenings (Equation (26)) and compression forces in the beams due to the PT force and column restraint (Equations (6)–(7)).

5. TWO-BAY BY FIRST-STORY PT FRAME TEST

To evaluate the effects of column restraint on the frame expansion and damage progress of the frame, a full-scale, two-bay by first-story PT frame (marked in Figure 2(b)) was cyclically tested. The tested frame as shown in Figure 12 had a column height H of 5.66 m and a beam span of 5 m. Each RC column (650×650 mm) was PT to a foundation using four 36-mm diameter high-strength bars (Table I(a)); longitudinal reinforcing bars were stopped before the base-to-footing interface. Instead of using transverse reinforcement in the beam-to-column connections, an A36 steel jacket was provided to confine the concrete in connections and RFPs were shop welded along the perimeter of the jacket and bolted to the steel beam ($H500\times200\times10\times16$) after post-tensioning the beams to the columns. A total of 12 ASTM A416 Grade 270 strands with each with a diameter of 15 mm were passed along beam webs, through three columns, and anchored outside exterior columns CL and CR. The initial PT forces in the columns and beams in each test are listed in Table IV.

5.1. Test loading

Each column (Figure 12) was extended to the mid-height of the second story, at which two 1000-kN actuators (Act 1 and Act 2) were positioned between the reaction wall and the frame and one 1000-kN actuator (Act3 or Act 4) was positioned in each beam span. A quasi-static cyclic loading with

DOI: 10.1002/eqe

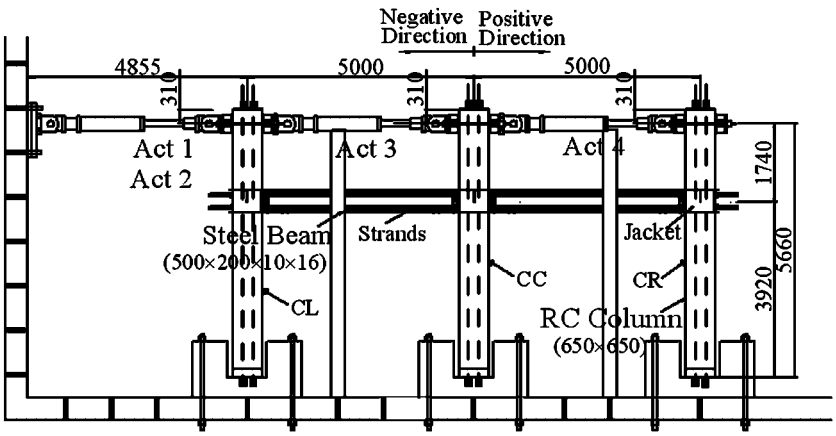

Figure 12. Tested frame (unit: mm).

Table IV. Initial PT force in the tested frame.

Test No.	Column Restraint	RFP	CL (kN)	CC (kN)	CR (kN)	Beam (kN)
1st	Minor	Yes	1075	1133	1130	916
2nd	Minor	Yes	947	1010	1036	868
3rd	Minor	No	933	996	1014	840
4th	Full	No	915	963	1035	793

increasing displacement amplitude was adopted for all the tests. Center column (CC) displacement at the loading point was controlled as a target displacement; the interstory drift was defined as the horizontal displacement at this loading point divided by the column height of 5.66 m. The displacement history consisted of three cycles of interstory drift with amplitudes of 0.25, 0.375, 0.5, 0.75, and 1%, followed by two cycles of drift with amplitudes of 1.5, 2, 3, and 4%. Two loading schemes were adopted in the test program. In the first loading scheme, the forces in Act 3 and Act 4 were slaved to three-quarter and one-quarter, respectively, the total forces in Act 1 and Act 2. Therefore, the shear force applied to columns CL and CR was half that applied to column CC at the loading point. Since the exterior column tops could expand with respect to center column CC, column restraint to the beam was minimal. This loading scheme was carried out for the first three tests (Table IV), in which RFPs used to increase connection energy were only included in the first two. For the second loading scheme, relative lateral deformation between column tops was excluded to simulate the pin-supported boundary condition, producing full restraint to the beam (4th Test). No energy dissipation devices were provided at column bases in all tests.

5.2. Test results

The first test was stopped at an interstory drift of 2% due to bending of the beam flange near the compression toe (Figure 13(a)) while the gap opened on the other beam flange. This failure mode, which resulted in loss of the initial beam strand force by 13%, was never observed in prior beam-to-column connection tests [10, 13]. Vertical stiffeners were welded to the beam flange inner side and web to reinforce the beam compression toe, so the frame could be retested. Two out of eight

DOI: 10.1002/eqe

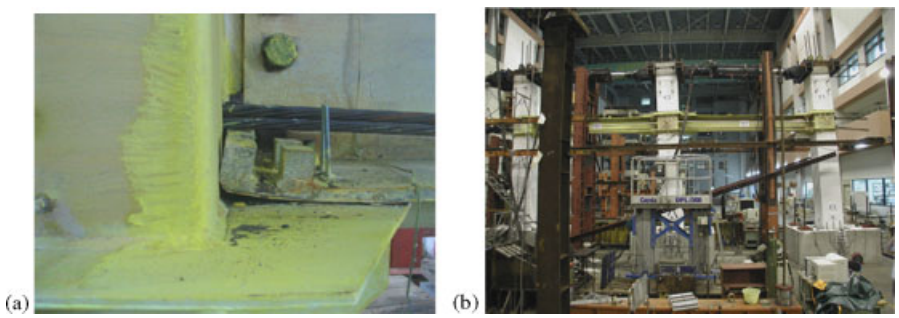

Figure 13. Observed performance in PT frame tests: (a) bending of beam flange (1st Test) and (b) deformation at a 4% drift (1st Test).

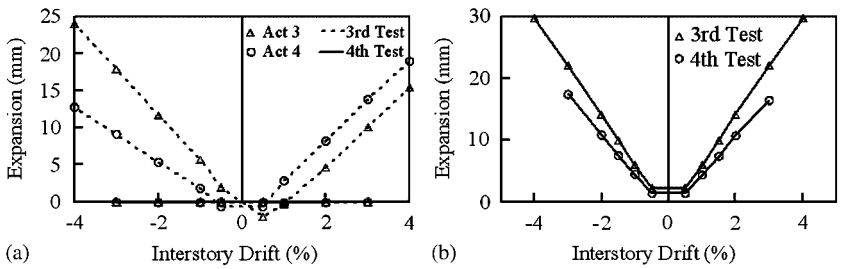

Figure 14. Actuator and frame expansion: (a) actuator expansion and (b) frame expansion.

RFPs fractured when the frame moved towards an interstory drift of 4% (Figure 13(b)). The frame was retested using the same loading protocol and no more RFP fractures occurred during the 2nd test. Six RFPs were removed from the connection after the 2nd test to evaluate the frame response in the 3rd test without ED devices. In the 4th test, the PT frame was loaded with no relative column deformation at actuator level, leading to zero deformation in Act 3 and Act 4 (Figure 14(a)). Conversely, these actuators in the 3rd test expanded due to gap-opening at the beam-to-column interfaces. Because column restraint was greater in the 4th test than in the 3rd test, the post-yielding stiffness of the PT frame was 20% higher in the 4th test than in the 3rd test (Figure 15(a)). The 4th test was stopped after the frame finished 3% drift cycles because Act 3 reached near the tensile capacity (1000 kN). Minor yielding of the beam web near the termination of the flange reinforcing plate was observed, and no buckling of the beam was observed after the 4th test.

5.3. Beam compression load

Figure 16(a) shows a deformed PT frame after gaps open at the column bases and beam-to-column interfaces. The RFPs are omitted for clarity. Notations T_{cl}, T_{cc}, and T_{cr} in the figure represent column PT forces, which are measured from load cells during tests. Notations A_l and A_r represent the actuator forces in Act 3 and Act 4, respectively, and P represents a total actuator force of Act 1 and Act 2. Notations V_{bl} and V_{br} represent the beam shear forces at the compression toes in beams BL and BR, respectively. Notation R with subscripts stands for the horizontal and vertical forces at each column base. Given the horizontal and vertical force equilibriums in the three columns and

DOI: 10.1002/eqe

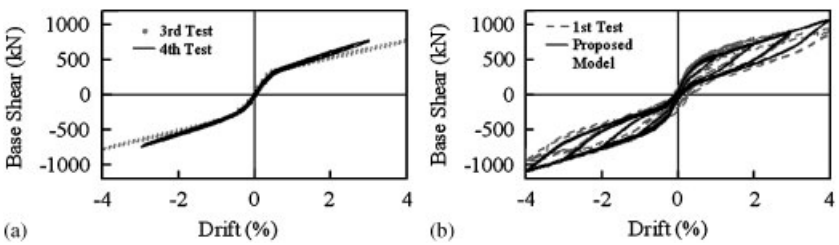

Figure 15. Hysteretic responses of PT frame tests: (a) 3rd and 4th Tests and (b) 1st test versus model prediction.

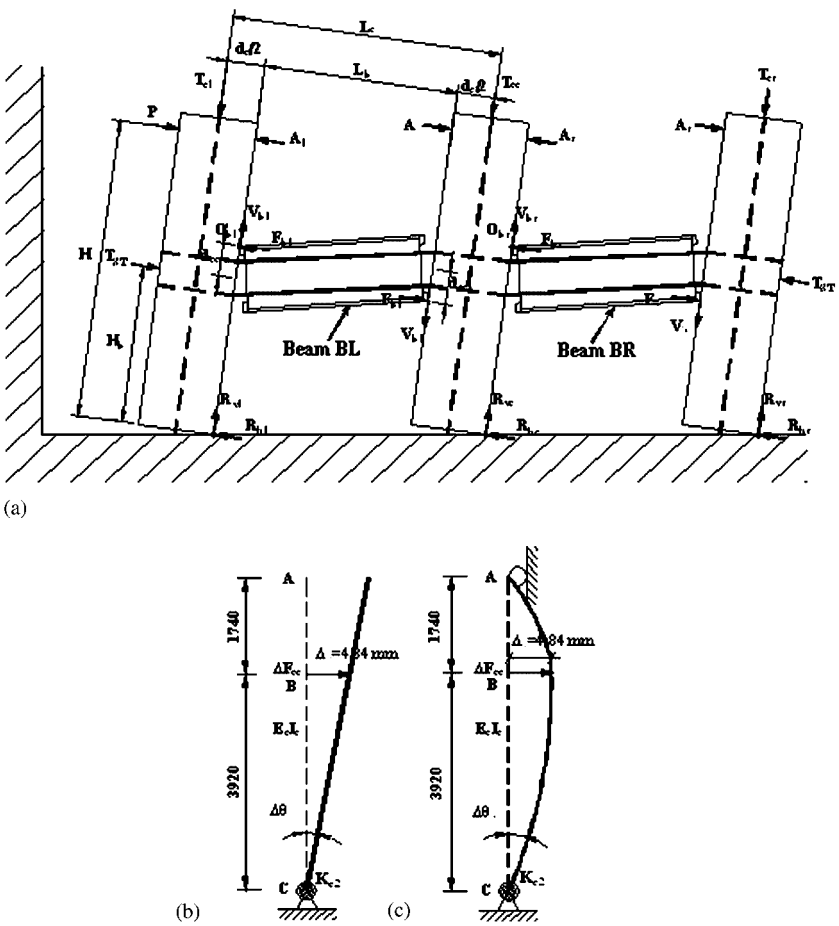

Figure 16. One-story PT frame and exterior column deformation: (a) one-story PT frame deformation; (b) column deformation (3rd Test); and (c) column deformation (4th Test).

DOI: 10.1002/eqe

Table V. Rotational stiffness K_{re} and K_{gcl}.

	Beam						Column	
	BL	BR	BL	BR	BL	BR	CL	CL
3% Drift	F_{bl} (kN)	F_{br} (kN)	ΔF_{cl} (kN)	ΔF_{cr} (kN)	K_{re} (kN m)	K_{re} (kN m)	$\Delta\theta_{gc}$ (rad)	K_{gcl} (kN m)
3rd Test	1453	1448	15	10	152	102	0.004	3585
Analysis	1425	1412	20	7	203	71	0.003	2689
4th Test	2040	1802	766	556	7732	5657	0.0082	7349
Analysis	2035	1885	715	565	7274	5748	0.0073	6542

the moment equilibriums at points O_{bl} and O_{br}, the compression forces in beams BL and BR are

$$F_{bl} = \frac{1}{H_b + d_{cc}} \left[(P - A_l) H + T_{ST} H_b - T_{cl} \frac{d_c}{2} \right] \tag{27}$$

$$F_{br} = \frac{H_b - d_{cc} - 2 d_{cc} d_c / L_b}{H_b + d_{cc}} F_{bl} + \frac{H(A_l - A_r)}{H_b + d_{cc}} - \frac{d_c T_{cc}}{2(H_b + d_{cc})} \tag{28}$$

where L_b is the clear beam span, H_b is the height of the beam centerline, H is the column height and $d_{cc} (= d_b/2 - t_f)$ is the distance between the beam centerline and the compression toe. In Tests 3 and 4, Table V shows the compression forces F_{bl} and F_{br}, calculated based on Equations (27) and (28). The incremental-restraining forces ΔF_{cl} and ΔF_{cr} are obtained by subtracting the strand force from the beam compression force. The rotational stiffness K_{re} is computed by substituting the incremental-restraining force, which is represented as $K_b \delta_{cc}$, and the measured gap-opening angle θ_g into Equation (24). The difference of gap-opening angles in columns CL and CC represents the additional gap-opening angle $\Delta\theta_{gc}$ due to the frame expansion. The rotational stiffness K_{gcl} is computed based on Equation (25) using the measured angle $\Delta\theta_{gc}$, the rotational stiffness K_{c2} of a SC spring [Equation (2)] and the gap-opening angle θ_g of the center column. Table V shows that the stiffness K_{re} and K_{gcl} is much higher in the 4th test than in the 3rd test, indicating that the high column restraint in the 4th test decreased the frame expansion between two exterior columns (Figure 14(b)) and also reduced the beam strand force increment (Figure 17). At a 3% drift, the beam strand tensile force was 612 and 432 kN greater in the 3rd and 4th tests, respectively, than the initial strand force. Figure 17 also shows that the beam compression force was similar to the beam strand force in the 3rd test but 60% greater than the beam strand force in the 4th test during which the distance between column tops was fixed. Following the same procedure described in the previous section, Figures 16(b) and (c) show deformed column shapes to determine column bending stiffnesses K_{cc}, which were 862 and 73366 kN/m for the 3rd and 4th tests, respectively. After substituting K_{cc} for K_{cl} and K_{cr} in Equations (18)–(20) to determine beam shortening components, the resulting beam compression forces were consistent with the test results (Figure 17). The cyclic response of the tested frame modeled based on the proposed rotational spring scheme was also close to that in the first test (Figure 15(b)). Note that the strength was overestimated after a 3% drift due to RFP fractures, which were not considered in the model.

DOI: 10.1002/eqe

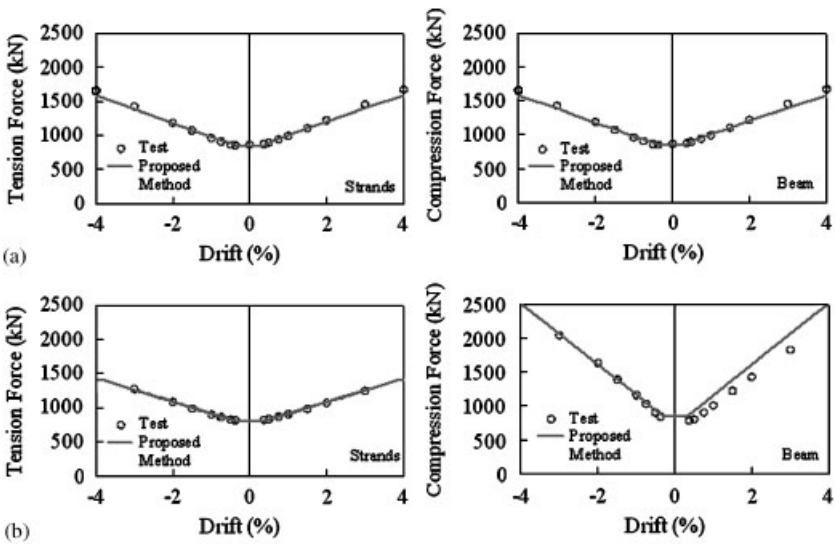

Figure 17. Strand tension force and beam compression force (one-story PT frame): (a) 3rd Test and (b) 4th Test.

6. CONCLUSIONS

This work presents an analytical method for evaluating the effects of column restraint resulting from gap-openings at beam-to-column interfaces in a post-tensioned self-centering moment frame. The procedure considers the following: (1) determining the column deformation in accordance with specified lateral displacements Δ_b at all beam-to-column interfaces along the column height, (2) computing the column bending stiffness at each story by the reaction force divided by the specified lateral displacement, and (3) computing beam shortenings (Equations (18)–(20)) and compression forces (Equations (21)–(23)) based on specified Δ_b. Because the column bending stiffness is obtained by a deformation that matches the frame expansion (Figure 7), the beam compression force estimate is more accurate than that calculated based on a pin–pin-supported column boundary condition. The predicted beam compression force is validated by a cyclic analysis of a three-story PT frame, which is modeled with numerous axial springs in connections to capture the gap-opening behavior, and by cyclic tests of a full-scale, two-bay by first-story PT frame, which represents a substructure of the three-story PT frame. The following conclusions are based on analytical studies and experimental results.

(1) For the three-story PT frame model subjected to cyclic loads, beam compression force exceeded strand force by 11% at the 1st story but was slightly smaller than the strand force at the 2nd and 3rd stories due to column deformation compatibility. The proposed procedure predicts beam compression force with reasonable accuracy. However, the simple estimation method based on the pin-supported column boundary condition at the upper story to determine column bending stiffness always predicts the increased compression force in the beam and overestimates beam compression forces in the 1st and 2nd stories by about 50%. The reason for this overestimation is that the worst-case scenario where a structure responds with a high drift at one floor while the

DOI: 10.1002/eqe

drifts in the floors above and below are near zero is adopted in an earlier approach [4, 8] but does not apply to a low and mid-rise PT frame.

(2) The full-scale, two-bay by first-story PT frame indicated by a dashed line in Figure 1(b), was cyclically tested. Two loading schemes were conducted on this frame to evaluate column restraint to the PT beams. The first loading scheme showed that the shear forces in exterior columns CL and CR were half that applied to center column CC to simulate a minimal column restraint. The second loading scheme resulted in no relative lateral deformation between all column tops when simulating a pin-supported boundary condition. The two loading schemes revealed different beam compression forces; the beam compression force was 2 and 60% greater than the strand tensile force in the first and second loading schemes, respectively. This verifies that the pin-supported condition at the upper story column significantly increases column bending stiffness and beam compression force, which is inconsistent with an actual PT frame structure subjected to cyclic loads.

(3) The self-centering behavior of the PT frame was modeled by incorporating three zero-length rotational springs at connections to describe the self-centering behavior, bilinear elastoplastic behavior and column-restraint behavior. This modeling technique that required fewer nodes and elements to model PT connections than the axial spring scheme could also predict test results well.

The proposed method using a deformed shape of columns to assess the restraining effect of columns was validated by a three-story PT frame, which responds in its first mode predominantly. It is expected that a higher mode affects the seismic response of taller structures and a future study is needed to derive appropriate deformed shapes of columns in assessing the column restraint in high-rise PT frames.

ACKNOWLEDGEMENTS

The test program is supported by the National Center of Research on Earthquake Engineering (NCREE), Taiwan with Prof. K. C. Tsai as the program director. The writers are grateful to Prof. H. L. Hsu of National Central University and Dr K. C. Lin of NCREE for their corporation on the design and construction of the test frame.

REFERENCES

1. Ricles JM, Sause R, Garlock MM, Zhao C. Posttensioned seismic-resistant connections for steel frames. *Journal of Structural Engineering* 2001; **127**(2):113–121.
2. Christopoulos C, Filiatrault A, Uang CM, Folz B. Posttensioned energy dissipating connections for moment-resisting steel frames. *Journal of Structural Engineering* 2002; **128**(9):1111–1120.
3. Garlock MM, Sause R, Ricles MJ. Behavior and design of posttensioned steel frame systems. *Journal of Structural Engineering* 2007; **133**(3):389–399.
4. Christopoulos C, Filiatrault A, Uang C-M. Self-centering post-tensioned energy dissipating (PTED) steel frames for seismic regions. *Report No. SSRP-2002/06*, Department of Structural Engineering, University of California, San Diego, CA, 2002.
5. Garlock M. Full-scale testing, seismic analysis, and design of post-tensioned seismic resistant connections for steel frames. *Ph.D. Dissertation*, Civil and Environmental Engineering Department, Lehigh University, Bethlehem, PA, 2002.
6. Chou C-C, Tsai K-C, Chen J-H, Chen Y-C, Chuang S-C. Cyclic behavior of post-tensioned steel connections with reduced flange plate and slab. *First International Conference on Advances in Experimental Structural Engineering*, Nagoya, Japan, 2005.

DOI: 10.1002/eqe

7. Kim HJ. Self-centering steel moment resisting frames with energy dissipating systems. *Ph.D. Thesis*, University of Toronto, Canada, 2007.
8. Kim HJ, Christopoulos C. Seismic design procedure and seismic response of post-tensioned self-centering steel frames. *Earthquake Engineering and Structural Dynamics* 2008; **38**(3):355–376.
9. Kim HJ, Christopoulos C. Numerical models and ductile ultimate deformation response of post-tensioned self-centering moment connections. *Earthquake Engineering and Structural Dynamics* 2008; **38**(1):1–21.
10. Chou C-C, Wang Y-C, Chen J-H. Seismic design and behavior of post-tensioned steel connections including effects of a composite slab. *Engineering Structures* 2008; **30**:3014–3023.
11. Chou C-C, Tsai K-C, Yang W-C. Self-centering steel connections with steel bars and a discontinuous composite slab. *Earthquake Engineering and Structural Dynamics* 2009; **38**(4):403–422.
12. Christopoulos C, Filiatrault A, Uang C-M. Shake table testing of a steel moment frame assembly with post-tensioned energy dissipating connections. *Proceedings of 7th U.S. National Conference on Earthquake Engineering*, Boston, MA, 2002.
13. Chou C-C, Chen J-H, Chen Y-C, Tsai K-C. Evaluating performance of post-tensioned steel connections with strands and reduced flange plates. *Earthquake Engineering and Structural Dynamics* 2006; **35**(9):1167–1185.
14. Chou C-C, Wu C-C. Performance evaluation of steel reduced flange plate moment connections. *Earthquake Engineering and Structural Dynamics* 2007; **36**(14):2083–2097.
15. Chou C-C, Lai Y-J. Post-tensioned self-centering moment connections with beam bottom flange energy dissipators. *Journal of Constructional Steel Research* 2009; **65**(10):1931–1941.
16. Collins JH, Filiatrault A. Application of post-tensioned energy dissipating (PTED) connections in steel moment-resisting frames. *Report No. SSRP-2003/05*, Department of Structural Engineering, University of California, San Diego, CA, 2003.
17. IBC. International Building Code. International Code Council, Falls Church, Virginia, 2000.
18. Tsai K-C, Lin B-Z. Development of an object-oriented nonlinear static and dynamic 3D structural analysis program. *CEER/R92-04*, Center for Earthquake Engineering Research, National Taiwan University, 2003.

DOI: 10.1002/eqe